DOI: http://dx.doi.org/10.22104/ijhfc.2016.212

Iranian Journal of Hydrogen & Fuel Cell 3(2015) 181-196

Iranian Journal of Hydrogen & Fuel Cell

IJHFC

Journal homepage://ijhfc.irost.ir

Numerical analysis of reactant transport in novel tubular polymer electrolyte membrane fuel cells

Akbar Mohammadi-Ahmar[1], Mohammad-Reza Elhami[2], Behzad Osanloo[3,*]

[1] School of Mechanical Engineering, College of Engineering, University of Tehran, Tehran, Iran
[2] School of Mechanical Engineering, College of Engineering, University of Imam Hossein, Tehran, Iran
[3] School of Mechanical Engineering, College of Engineering, University of Tabriz, Tabriz, Iran

Article Information

Article History:

Received:
01 December 2015
Received in revised form:
27 January 2016
Accepted:
01 February 2016

Keywords

CFD
PEM fuel cell
Novel tubular architectures
Current density
Reaction surface.

Abstract

In the present work, a numerical analysis of three novel PEM fuel cells with tubular geometry was conducted. Three different cross sections were considered for the PEM, namely: circular, square and triangular. Similar boundary and operational conditionswere applied for all the geometries. First the obtained polarization curve for basic architecture fuel cells was validated with experimental data and then the results of the three novel tubular architectures were compared with basic conventional geometry. The results showed that for the case of V=0.4 volts, circular and square tubular models gives up to 27.5 and 8 percent outlet current density more than the base model, whereas the triangular model predicts a decrease of 14.37 percent compared to the base model. Because the square tubular and in particular the circular tubular models do not have sharp edges, uniform reactioncan take place over the entire catalyst layer of the cathode and anode electrodes, and therefore the distribution of the hydrogen, oxygen and water is uniform. Also, circular geometry, due to use of all the reaction surface and lack of dead zones, produces higher power outputs. The temperature distribution in a lateral direction in the reaction zone for all three configurations indicates that the maximum temperature for the circular tubular has the lowest values in comparison to the other two cases, which results from a uniform surface reaction for this geometry. The results presented in this paper can be used for designing novel architecture of fuel cells.

1. Introduction

Recent advances in the fields of modern technology have had a significant impact on increasing demand for energy. With the increase in demand, more people are turning to the use of limited energy resources and searching for alternative forms of energy that not only cause no harm to the environment but also help reduce pollution. One of these methods which develops electrical energy with high efficiency without creating

*Corresponding Author's E-mail address: b_osanloo91@ms.tabrizu.ac.ir

environmental and acoustic pollution is fuel cells, which utilize a direct combination between fuel and oxidization. Among the different types of fuel cells (such as alkaline, direct methanol, solid oxide, and molten carbonate) the proton exchange membrane fuel cell (PEM) is one of the most functional fuel cells and is applied in different sectors of transportation and housing. Proton exchange membrane fuel cell (PEM) can be a good alternative to other energy convertors due to their simplicity of design, storage, efficiency and quick set up [1-3]. PEM fuel cell experimental research has only offered general parameters such as polarization characteristic in different current density by examining the current-voltage curve. Unfortunately, a thorough understanding of the species transport within the PEM fuel cell is not possible due to size limitations of the device. PEM fuel cell performance not only includes the electrochemical reactions, but also current distribution, fluid mechanics, species transport, managing heat and water. Using experiments to understanding these complex electrochemical reactions and new reactants transport restrictions is difficult and often impossible. However, PEM fuel cell modeling provides a better understanding of such electrochemical reactions and transport phenomena. The purpose of such modeling is to determine the best methods to achieve maximum power and reduce losses in PEM fuel cells. In this regard, some of the previous studies have dealt with examining environmental effects such as rising temperature, pressure and inlet humidity of the reactants on the outlet power of PEM fuel cells and have concluded that such an increase in the parameters have a significant impact on PEM fuel cell performance [4-8]. But in practice, such changes in fixed environmental conditions is energy consuming and therefore not economically viable.

Moreover, the effects of materials used in PEM fuel cells, like porosity, diffusion coefficient, absolute permeability and membrane phase conductivity, has been evaluated in other studies [5, 9-11]. In fact because of limitations in the choice of materials, the use of such methods for increasing the power is accompanied with some difficulties. Other works have examined the geometric parameters such as thickness of the Gas Diffusion layer, Catalyst layer and membrane, changing the channel cross-section, making the channels convergent or divergent, creating different obstacles including the baffle, and different pin configurations inside the channel of the PEM fuel cell. For example, Burning and Djilali examined the effect of geometric and material parameters, such as thickness and porosity coefficient of the GDL, on the performance of fuel cells [12]. They concluded that at low current densities increasing the thickness of the GDL leads to an increase in average mass fraction of oxygen due to more lateral dispersion of the thicker GDL.The effect of three-dimensional configurations of the channel, including rectangular, trapezoidal and parallelogram cross sections, was simulated by using a non-isothermal model in a straight single channel PEM fuel cell by Ahmed and Sung [13]. Simulations showed that the channels with a rectangular cross section results in higher cell voltages compared to the other two cross-sections. Although the channel with trapezoidal cross-section facilitates the distribution of the reactants, Yan et al. [14] proceeded to examine the impact of channel convergence in vertical and lateral directions in order to improve the efficiency of PEM fuel cells. They reduced flow channels with different width and height taper ratios to compare the fuel transport characteristics to channel with a constant cross-section. They found that by converging the channel in the lateral direction and diverging it in the vertical direction cell performance improves. In addition, Fontana et al. [15] dealt with the effect of channel convergence angle in increasing outlet power and pressure drop along the channel. They examined the three angles of convergence i.e. 0.25, 0.5 and 0.75 degrees, and found that a 0.75 degrees angle and the channel with a constant cross section gives greater current density increasing the over pressure drop by a factor of 3.5 as compared to the other angles. Perng and Wu [16] dealt with a three-dimensional numerical simulation of a single channel PEM fuel cell using the trapezoidal baffles within the cathode and anode channels. By changing the angle and height of the baffles and comparing the results within the channels

they found that novel gas channel with trapezoid baffles, increases the net output power by about 90%. It is noteworthy that each of these methods increased the power but reduced the non-uniform distribution of temperature, current density and low distribution of the reactants in the catalyst layers, these results indicate that novel architectures for PEM fuel cell are needed. Some examples of the small amount of work done in the recent years in this area include the following studies. Al-Baghdadi and Maher [17] compared the performance of a novel tubular PEM fuel cell with a conventional planar PEM fuel cell. They concluded that the tubular architecture presents a better performance for the current density and the reactants transport, and also provides a higher current density. Also, in novel PEM fuel cell architecture the effect of geometric parameters and materials have been evaluated. Most recently, Soria et al. [18] evaluated the performance of three flow fields with cylindrical architecture including the serpentine, interdigitated and straight channel in the PEM fuel cells. Their results showed that configurations with cylindrical channels reduce the pressure drop due to gradual reduction of the angle of the flow path, thereby facilitating the expulsion of liquid water from gas diffusion layers. Torkavannejad et al. [19] investigated three novel architectures of single cell proton exchange membrane fuel cells, namely circular, square and octagonal duct-shaped architectures, under isothermal conditions and steady state. They found that square and circular architectures showed a significantly better performance. They stated that the geometry with a square cross-section shows more current density and more uniform temperature, and water distribution is the best alternative for the production of novel fuel cell architectures. So, in the present paper three novel configurations for a PEM fuel cell consisting of (a) circular tubular, (b) rectangular tubular and (c) triangular tubular have been proposed to indicate the improvement in the results. To indicate the improvement in the results, simulation of the basic architecture fuel cell has been done and the obtained results have been validated by Wang et al.'s experimental results.

2. Description of the computational model

Figs. 1 and 2 show the grid and computational domain along with the boundary condition for the base and three tubular models, respectively. The new models studied in the present work consist of three tubular geometries with circular, square and triangular cross-sections. Each of these figures include gas diffusion layers (GDL), the catalyst layers (CL), membrane (MEM) and electrode layers (EL). A feature of these new models is increasing reactants distribution which leads to an increased reaction surface. Another feature is the entire surface of the electrode is used for electron transfer which is why the increase in power density is expected compared to the basic architecture for the fuel cell reaction compared to the base model where only the horizontal surfaces (electrode plates) of the flow is used. In the present study a parallel flow, non-isothermal, single-phase and three-dimensional model is used for solving computatinal fluid dynamic equations in the three novel tubular architectures of PEMFC.

Boundary conditions in these new architectures are similar to the basic PEM fuel cell. The present simulations were performed in order to achieve accurate results and ensure that the obtained results are independent of the grid. The parameter used for this work was the current density. Finally, the hexahedral grids used in these models for tubular with circular, square and triangular cross sections were 408000, 666400, and 599760, respectively. The computational region and structured grid used for these new architectures are presented in Fig. 2.

2.1. Model assumptions

Assumptions used in the model simulation, includes the following cases:

(1) It operates under steady state. (2) Inlet gas mixture is an incompressible ideal gas. (3) Due to pressure gradients and low flow velocity, flow in the channels is laminar. (4) The gas diffusion and catalysts layers and membrane in porous zones are homogeneous and isotropic. (5) There are non-isothermal and steady

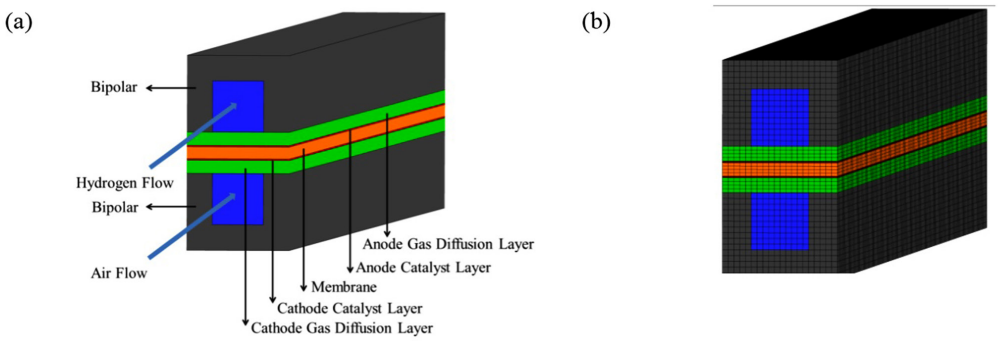

Fig. 1. (a) Computational region, boundary conditions and (b) grid, for the base model.

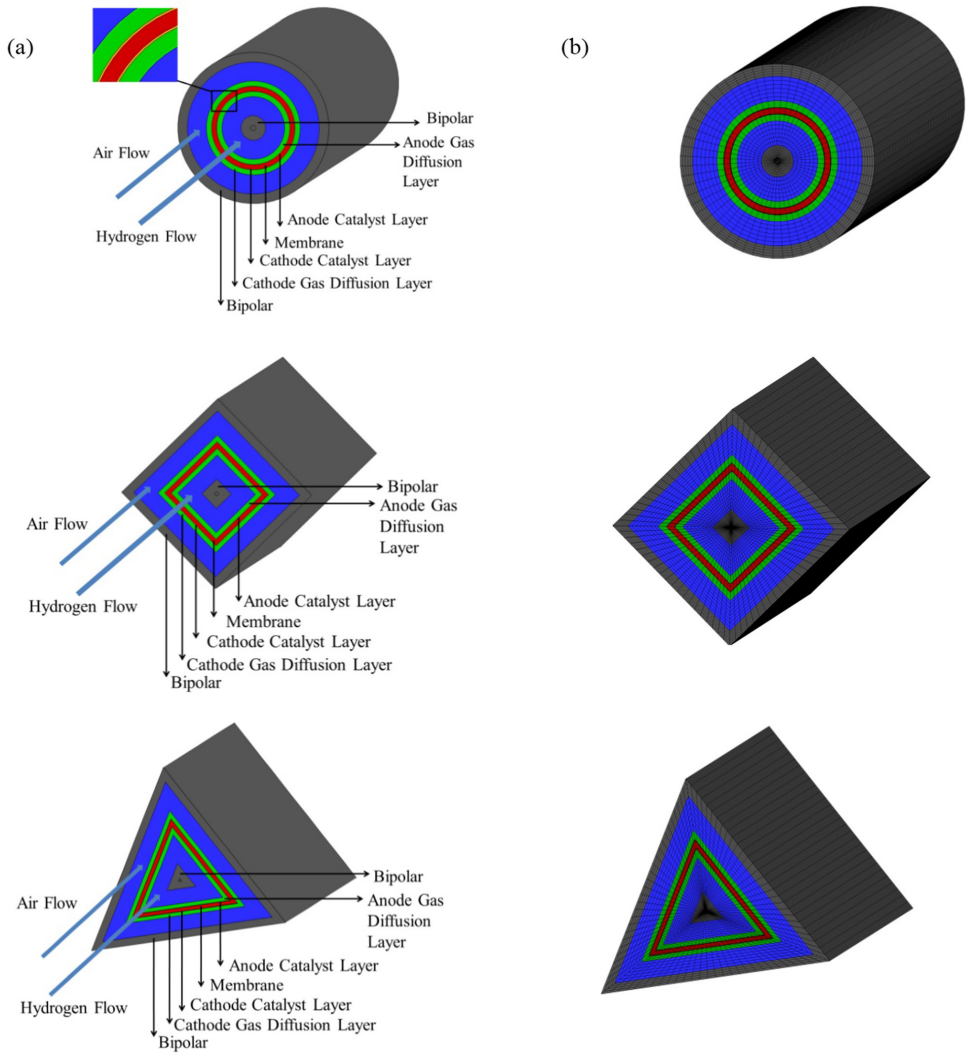

Fig. 2. (a) Computational region, boundary conditions and (b) grid used in the three novel cylindrical models.

state conditions. (6) Electrochemical reactions take place on surfaces of the catalyst layers. (7) Liquid water transport in the membrane are controlled by diffusion and osmotic drag mechanisms. (8) Diffusion of species and electrochemical reaction are based on the dilute solution theory and Butler-Volmer kinetic equation, respectively. (9) At the inlet, fully humid conditions are considered for the anode and cathode. (10) The amount of the liquid phase water produced from chemical reactions is small and phase changes or two phase transports have not been considered. This could be a model for future work and it will be investigated.

2.2. Governing Equations

Transport phenomena that occur inside a PEM fuel cell are expressed by governing equations including conservation of mass, momentum and transport of the charge and species. These equations can be described as follows:

Continuity and momentum equations

$$\nabla.(\rho\mathbf{V}) = \mathrm{S_m} = 0 \tag{1}$$

Where ρ is the fluid density and $\mathbf{V}$ is the apparent velocity vector. The momentum equation in steady state is expressed as follows:

$$\nabla.(\rho\mathbf{V}\mathbf{V}) = -\nabla \mathrm{p} + \nabla.(\mu_{\mathrm{eff}}\nabla\mathbf{V}) + \mathrm{S_p} \tag{2}$$

Where $\mathbf{p}$ is the static pressure, μ_{eff} is the mixture of average viscosity, and $\mathrm{S_p}$ is the source term that contains the physical properties of the porous regions and is expressed as follows:

$$\mathrm{S_p} = -(\mu/K)\mathbf{V} \tag{3}$$

where K is the permeability of the gas diffusion layers and catalyst layers. μ is the gas viscosity and $\mathbf{V}$ is the apparent velocity vector in porous zones [21].

Species transporting equation:

To determine the local mass fraction of each component of y_i, species transport equation are applied as follows:

$$\nabla.(\rho\mathbf{V}\mathrm{y_i}) = -\nabla.(\rho(\mathrm{D_i}\nabla.\mathrm{y_i})) + \mathrm{S_i} \tag{4}$$

where $\mathrm{S_i}$ is the source term for each species and $\mathrm{D_i}$ is the diffusion coefficient for each species which are defined as follows:

$$\mathrm{S}_{H_2} = -\frac{M_{W,H_2}}{2F}R_{an} \tag{5}$$

$$\mathrm{S}_{O_2} = -\frac{M_{W,\mathrm{O_2}}}{4F}R_{cat} \tag{6}$$

$$\mathrm{S}_{H_2O} = \frac{M_{W,\mathrm{H_2O}}}{2F}R_{cat} \tag{7}$$

$$D_i = \varepsilon^{1.5}D_0\left(\frac{101325}{p}\right)\left(\frac{T}{300}\right)^{1.5} \tag{8}$$

Where D_0 is the component mass distribution in the reference temperature and pressure [21].

Energy equation

The temperature field is obtained by solving the energy equation as follows:

$$\nabla.(\mathbf{V}(\rho E + p)) = \nabla.(k_{eff}\nabla\mathrm{T} - \sum h_i(-\rho\,\mathrm{D}_i\nabla.\mathrm{y}_i)) \tag{9}$$

Where E is the total energy and h_i is the enthalpy of each species. The term $(-\rho\,\mathrm{D}_i\nabla.\mathrm{y}_i)$ is the flux diffusion for species i, which is calculated for a laminar flow. Also, k_{eff} is the effective conductivity coefficient representing the gas mixture thermal conductivity in hollow channels and in the membrane which were presented as follows:

$$k_{eff} = \frac{1}{\frac{1-\varepsilon}{3k_m} + \frac{\varepsilon}{2k_m + k_w} - 2k_m} \tag{10}$$

Where, k_m and k_w are the thermal conductivity of the membrane (Nafion) and water, respectively.

Electrochemical model

To account for the electron transport in of catalysts layer, gas diffusion layer and plates and also for transporting of protons through the membrane and catalyst layers, it is necessary to solve two equations to predict the electrochemical phenomena occurring in the PEM fuel cell as follows [21]:

$$\nabla.(\sigma_{sol}\nabla\varphi_{sol}) + \mathrm{R}_{sol} = 0 \quad (11)$$

$$\nabla.(\sigma_{mem}\nabla\varphi_{mem}) + \mathrm{R}_{mem} = 0 \quad (12)$$

Where σ is the ionic conductivity, φ is the cell potential and R is the convection currents. Also, the mem and sol subscripts correspond to the solid and the electrolyte phases. Using the Butler-Volmer`s general relation used for calculating the local current density in the catalyst layers, exchange current density is obtained as follows:

$$\mathrm{R}_{an} = J_{an}^{ref}\left(\frac{H_2}{H_{2,ref}}\right)^{\gamma_{an}}\left[\exp\left(\frac{\alpha_{an}F\eta_{an}}{RT}\right) - \exp\left(-\frac{\alpha_{cat}F\eta_{an}}{RT}\right)\right] \quad (13)$$

$$\mathrm{R}_{ca} = J_{cat}^{ref}\left(\frac{O_2}{O_{2,ref}}\right)^{\gamma_{cat}}\left[-\exp\left(\frac{\alpha_{an}F\eta_{cat}}{RT}\right) + \exp\left(-\frac{\alpha_{cat}F\eta_{cat}}{RT}\right)\right] \quad (14)$$

Where J^{ref} is the volumetric reference exchange current density and $H_2/H_{2,ref}$ and $O_2/O_{2,ref}$ are the reference and local species concentration on the anode and cathode, respectively, γ is the concentration coefficient, α is the transfer coefficient, F is the Faraday constant and η is the activation losses. Activation losses or local surface verpotential, η controls reaction. This parameter is associated with the potential difference between the electrodes and the electrolyte surfaces $(\varphi_{sol}, \varphi_{mem})$. This overpotential is calculated for both the anode and cathode sides and includes the open circuit voltage, V_{oc}.Therefore, the potential difference between the electrodes are established as follows:

$$\eta_{an} = \varphi_{sol} - \varphi_{mem} \quad (15)$$

$$\eta_{cat} = \varphi_{sol} - \varphi_{mem} - V_{oc} \quad (16)$$

Where V_{oc} is the open circuit voltage and is obtained from the following equation [22]:

$$V_{oc} = 0.0025T + 0.2329 \quad (17)$$

For a membrane which is modeled as a porous zone, Springer reported that the ionic conductivity, , and electro-osmotic drag coefficient is obtained as a function of water content as follows [24]:

$$\sigma_{mem} = (0.00514\lambda - 0.00326)\mathrm{e}^{1268(1/303 - 1/T)} \quad (18)$$

$$\lambda = 0.043 + 17.81a - 39.84a^2 + 36a^3 \quad (\mathrm{a} < 1) \quad (19)$$

$$\lambda = 14 + 1.4(a - 1) \quad (\mathrm{a} > 1) \quad (20)$$

where a is the water activity.

2.3. Boundary Conditions

The boundary conditions required for the computational domain are shown in Figs. 1 and 2. Inlet velocities at the entrance of the anode and cathode gas channels are calculated as the following [25]:

$$u_{in,a} = \frac{\xi_{an}\, I/(2F) A_{mem} M_{H_2}}{\rho_{H_2} A_a} \quad (21)$$

$$u_{in,a} = \frac{\xi_{in,cat}\, I/(4F) A_{mem} M_{O_2}}{\rho_{O_2} A_c} \quad (22)$$

Inlet velocities at the anode and cathode gas flow channels (in equations 21 and 22) for solving the momentum equation are obtained by the stoichiometric flow ratios, ξ_{an}, ξ_{cat}, PEMFC operating current density,I, the cross-sections area of the anode and the cathode, A_{an}, A_{cat}, and finally hydrogen and air density. Moreover, the cross-sections area of the anode and the cathode, , and finally hydrogen and air density.

Moreover, the same mass flow rate is applied at the inlet channels of the base model and the three tubular cases. Zero gauge pressure conditions at the outlet have been applied to the atmosphere for discharge simulation. Also, zero flow direction gradient has been established (Neumann boundary condition) for the other parameters. The non-slip boundary condition for velocity and coupled boundary condition and zero Species flux is determined at the interface between the fluid and non-porous solid walls. The temperature on the external surface of the bipolar plate is specified as cell operation ambient temperature in the present study.

2.4. Numerical methodology

At the present study, the finite volume method, SIMPLE algorithm in Ansys Fluent 14 software [21], is used to obtain the conservative form of the governing equations including convective, diffusion and source terms [26]. The algebraic multigrid method is used in order to speed up the convergence. Then calculation is done in more than one grid level by eliminating high errors and low frequencies. Second order upwind is used for the interpolation functions. In the multi-grid method, the F-cycle along bi-conjugate gradient stabilized method (BCGSTAB) is used. The most number of cycles is set to 60, along with one pre-sweep and two post-sweep steps. This computational process was finished when the relative error of each parameter reached for the specific convergent criteria. Other physical and current parameters are presented in Table 1 from the experimental data of Wang et al. [20]. These parameters have been used in both the base conventional model and three new configurations.

3. Results and discussion

To validate the present work the obtained results from the polarization curve for a base fuel cell with straight channels were compared with Wang et al.'s experimental data [20] in Fig. 3. The comparison shows that the present numerical simulation in a wide range of obtained values is in good agreement with the experimental results. However, at high current densities the numerical simulation shows a slight deviation from the experimental results. That is because the model in the numerical simulation removes liquid water, considered formed water, in the catalyst layer in the form of vapor phase. As liquid water fills the catalyst and gas diffusion layers and therefore prevents the oxygen molecules from reaching the catalyst surface. As shown in Fig. 3 (a) and (b), this factor led to the loss of species and eventually reduces power density compared with the experimental results.

Figure 4 shows the comparison of the performance of the three new architectures with the base conventional model fuel cell by polarization curve. As shown in Fig. 4(a), circular and square tubular configurations produced a higher current density compared with the base PEM fuel cell model. In contrast, the triangular tubular configuration shows a drop in current density especially in the low-voltage. These three novel configurations in high voltage values predict almost similar results, but with a reduction in cell voltage the circular tubular architecture shows more values compared to two other new figures due to a more uniform surface distribution. The corresponding power density also have been proposed for the three new architectures and base model in Fig. 4(b). According to Fig. 4(b), circular and square tubular architectures presented more power density compared with the basic architecture. While the triangular architecture, due to the surface non-uniform distribution, presented lower power density.

In order to interpret the results of the polarization curve more accurately, as shown in Fig. 4, contours of hydrogen mass fraction are presented for the three novel architectures in Fig. 5. The circular tubular configuration shows a more uniform distribution of hydrogen in comparison with the two other architectures and especially with the triangular tubular. Another point is that the range of value change of hydrogen in the catalyst and gas diffusion layers in the triangular tubular architecture is so wide that the corner zones have the maximum values due to

Table1 Physical Parameters and Boundary Conditions used in the Base Model and the Three Tubular Cases.

Parameter	Symbol	Value	Unite
Gas channel length	L	0.05	m
Gas channel height (base model)	H	0.001	m
Gas channel width (base model)	W	0.001	m
Land area width (base model)	W_L	0.001	m
Diffusion layer thickness	δ_{GDL}	0.26×10^{-3}	m
Catalyst layer thickness	δ_{CL}	0.029×10^{-3}	m
Membrane thickness	δ_M	0.23×10^{-3}	m
Gas diffusion layer porosity	ε_{GDL}	0.4	-
Membrane porosity	ε_M	0.4	-
Permeability	K	1.76×10^{-11}	m^2
Faraday constant	F	96485	C/mol
Anode pressure	P_a	3	atm
Cathode pressure	P_c	3	atm
Inlet fuel and air temperature	T_{in}	353	K
Fuel/air stoichiometric ratio	ξ_a/ξ_c	2/2	-
Relative humidity of inlet fuel and air (fully humidified conditions)	RH	100%	-
Electrode electronic conductivity	λ_e	100	S/m
Membrane ionic conductivity (humidified Nafion117)	λ_m	17.1223	S/m
Transfer coefficient, anode side	α_a	0.5	-
Transfer coefficient, cathode side	α_c	1	-
Electrode thermal conductivity	k_e	1.3	W/mK
Membrane thermal conductivity	k_m	0.455	W/mK
Membrane equivalent weight base model and three tubular cases)	-	1100	g/mol
H_2 diffusivity	$D_{H_2-H_2O}$	1.1×10^{-4}	m^2/s
O_2 diffusivity	$D_{O_2-N_2}$	3.23×10^{-5}	m^2/s
H_2O diffusivity at cathode	$D_{H_2O-N_2}$	7.35×10^{-5}	m^2/s
H_2O diffusivity at anode	$D_{H_2O-O_2}$	7.35×10^{-5}	m^2/s

the low flow velocity in these regions. All three new configurations have a higher overall reaction surface compared with the base PEM fuel cell, but the circular and square tubular configurations show a higher uniformity level compared with the triangular case.

Comparison of the oxygen mass fraction contours is presented in Fig. 6. The maximum value of oxygen is shown at the inlet of the computational region. Moreover as flow approaches the downstream due to the decreased amount of oxygen in the channel, its permeation into the gas diffusion layer and the catalyst layer decreases. Mass fraction of oxygen for square tubular and triangular tubular is maximum in the corners due to low flow velocity in these regions. Moreover, it is can be seen that the non-uniform distribution in the diffusion layer causes a reduction in reaction and thus reduces the current density. This non-uniformity of the oxygen consumption in triangular tubular architecture is high compared to two other cases.

Water mass fraction contours in the gas diffusion and catalyst layers at the cathode side are shown in Fig.7. Moving along the channel in the cathode side will increase the water content. This increase in the water

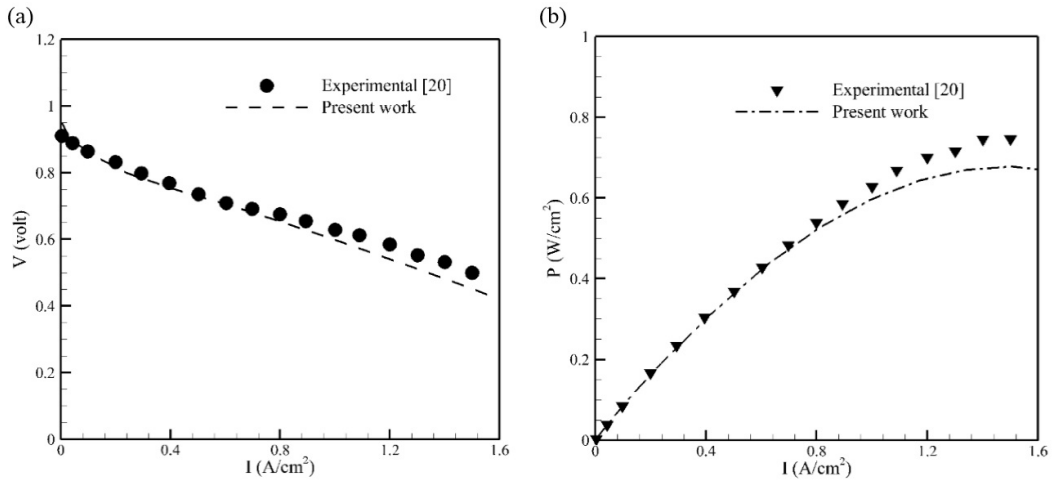

Fig. 3. Comparison of polarization curves between the base model predictions and experimental data [20].

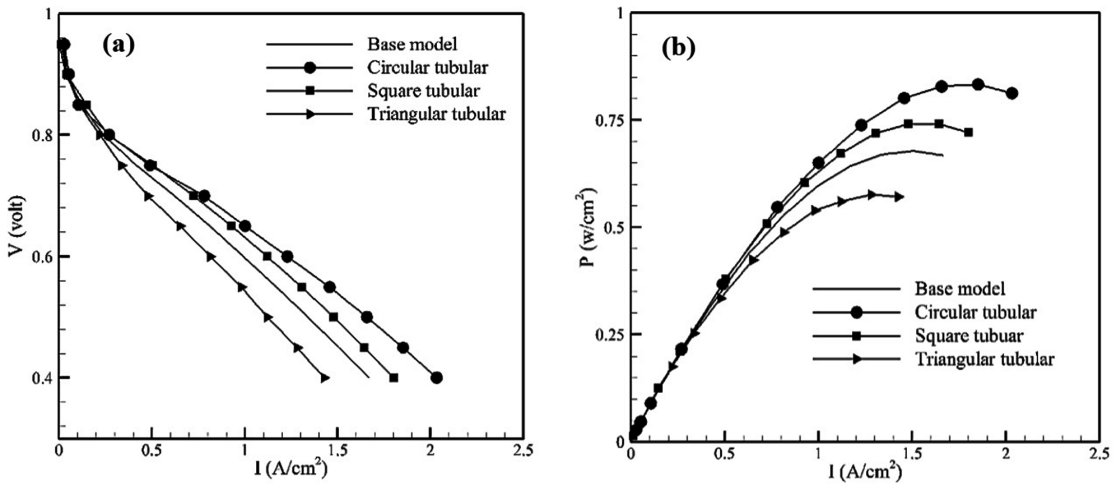

Fig. 4. Comparison of the results of different arrangements (a) current density (b) the power density.

amount is related to the phenomenon where water is produced by the electrochemical reaction along the channel and at the same time the water is transported from the anode to the cathode by electro-osmotic drag. Also, similar to previous contours, the triangular tube has the most non-uniformity. A lower concentration of water is predicted in the corners of the triangular architecture indicating the slowness of reaction in these regions. These regions have too little activity compared to other regions. Unlike this architecture, the circular tubular configuration shows a uniform distribution for water vapor due to the uniform distribution presented in the previous contours of the reaction species, consequently there is little difference between its maximum and minimum values. The square architecture is expressed between these two configurations, so power density is placed between the circular and triangular architectures. Therefore, the important result is that surface uniformity of fuel cell configuration has a direct effect on the amount of current density, and finally the outlet power density should be evaluated in designing new architectures of PEM fuel cells.

The contours of water vapor mass fraction shown in Fig. 8 can be used to determine the content of transposed water from the anode through electro-

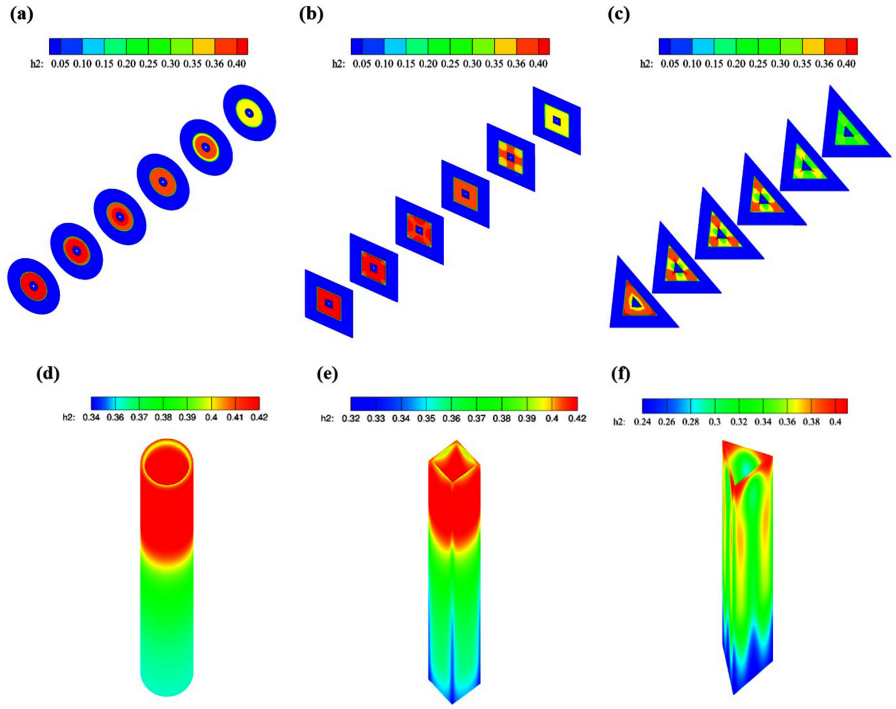

Fig. 5. Hydrogen mass fraction contours at , (a), (b), (c) the entire domains and (d), (e), (f) the gas diffusion and catalyst layers of the anode.

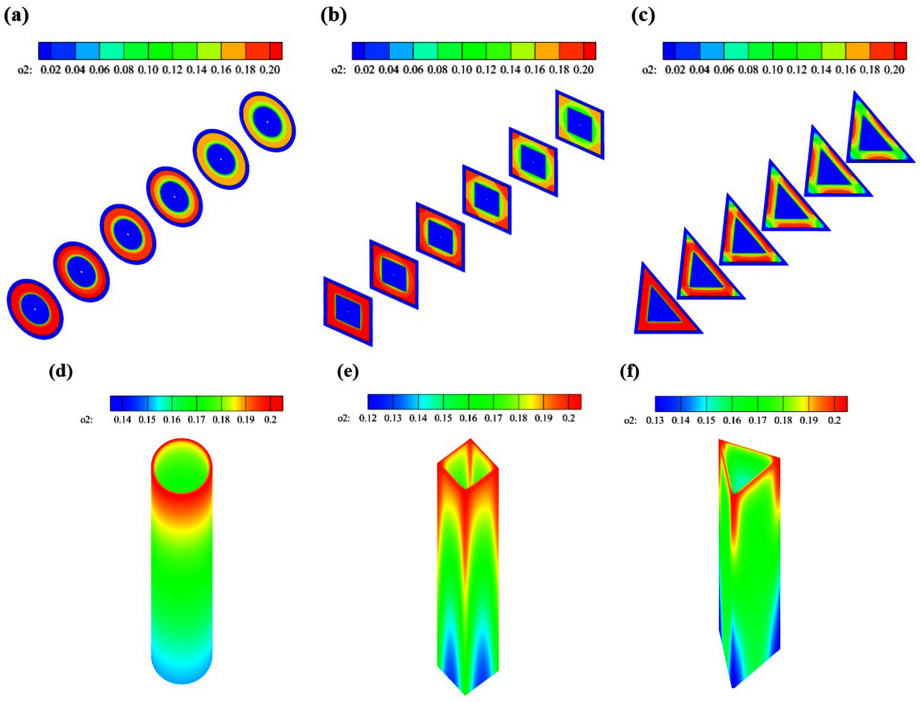

Fig. 6. Oxygen mass fraction contours at , (a), (b), (c) the entire domains and (d), (e), (f) the gas diffusion and catalyst layers of the cathode.

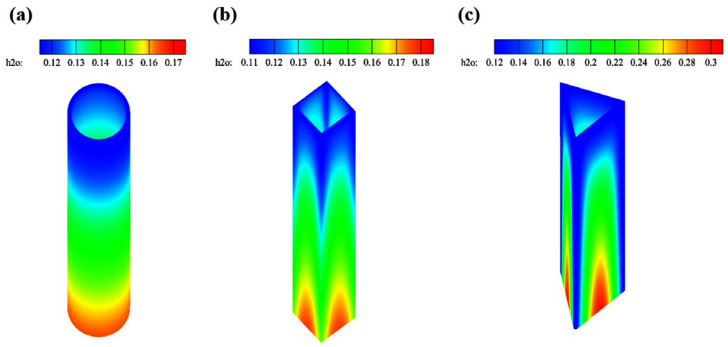

Fig. 7. Water mass fraction contours in the gas diffusion and the catalyst layers of the cathode at V=0.4 v.

osmotic drag toward the cathode for the three new architectures,. According to Fig. 8, the water along the channel gradually decreases for these three tubular architectures. In addition, the difference between maximum and minimum values of transported water increased for the triangular configuration.

Another important factor in designing the fuel cell is the control of increasing temperature and uniform temperature distribution in heat producing regions. Increasing temperature in PEM fuel cell is caused by heat produced by the heating nature of the general reactions of the cell, Joule heat and water phase change. The heat produced by the novel architectures was investigated by the temperature distribution contours presented in Fig. 9. As shown in Fig. 9, the maximum temperature occurs at the inlet region for all the architectures due to the small amount of water produced. By moving along the channel, water

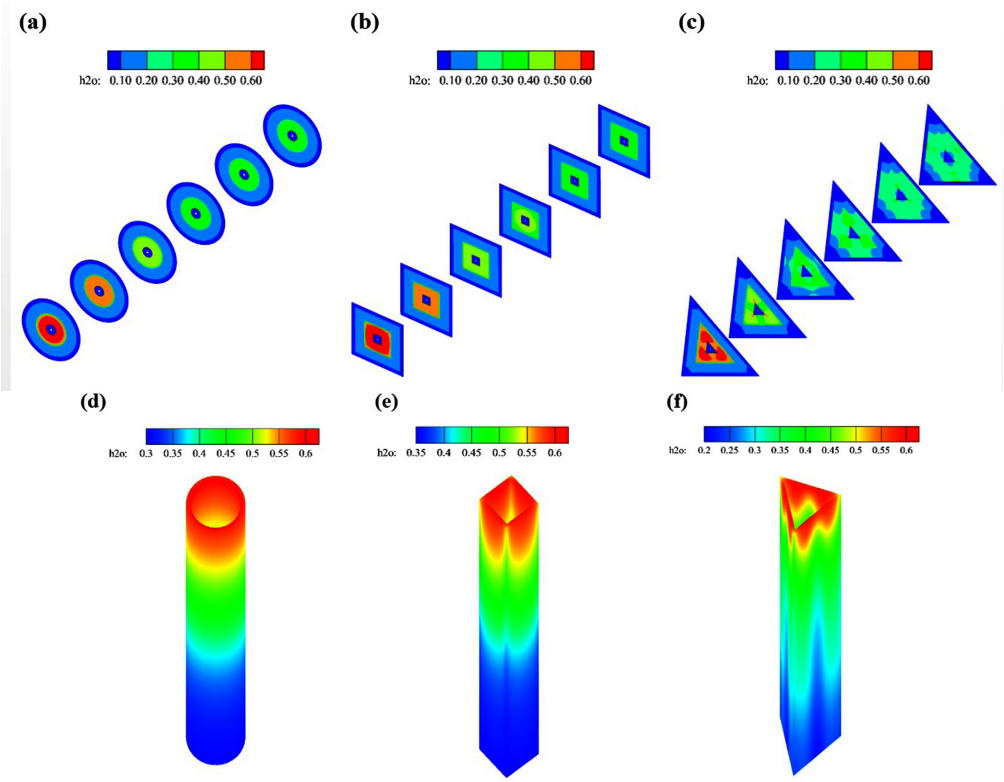

Fig. 8. Water mass fraction contours at , (a), (b), (c) the entire domains and (d), (e), (f) the gas diffusion and catalyst layers of the anode.

content increases and as a result the temperature gradually reduces. In the square and triangular tubular architectures, due to their sharp corners and slowness of the reaction, the temperature increase is concentrated in the regions away from the corner. There is no significant rise in temperature at the corners. This maximum temperature concentration can damage the membrane, gas diffusion and catalyst layers. It is most undesirable in the catalyst layer due to the cost. The maximum temperature is lower for the circular tubular architecture in comparison with the two other architecture due to species uniform distribution.

Figure 10(a) presents the temperature distribution in the enterance region. (the region where the maximum rise in temperature occurred) in the lateral direction. The results of the base geometry is also shown in Fig. 10(b). According to Fig. 10 (a) and (b), the peak temperature is nearly the same for the base and three new fuel cell membranes and catalyst layers. According to Fig. 10(a), as the reaction surface in the base model is reduced the maximum temperature is less compared with the novel geometries. On the other hand, the maximum temperature for the circular tubular configuration is less compared with the two other architectures, and the triangular configuration shows the greatest increase in temperature. Circular architecture had the widest range of increase in temperature due to distribution of the reaction at all surfaces and therefore has a lower amount of maximum temperature. But on the otherhand, the triangular architecture had the maximum temperature occurring in a limited area due to having sharp corners and non-uniform reaction. Therefore the maximum temperature for this configuration is high compared with the two other architectures, which causes dryness of the membrane at the anode and results in an increase of resistance against ion transport in the membrane. This factor should be utilized in the design of high temperature fuel cells along with the

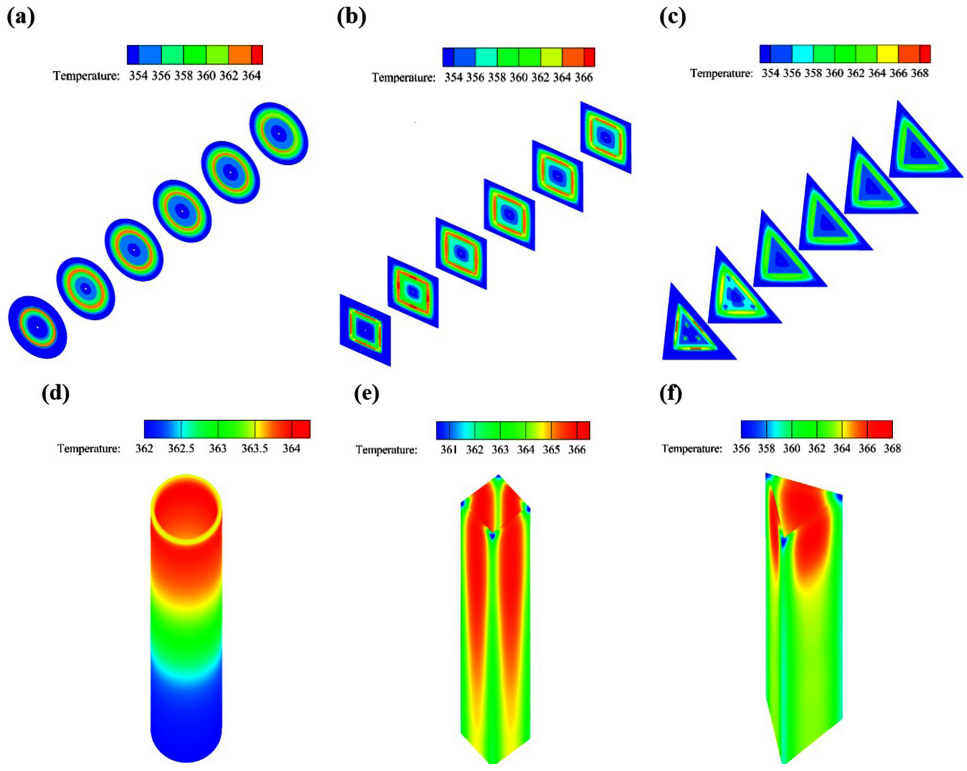

Fig. 9. Temperature distribution contours at , (a), (b), (c) the entire domains and (d), (e), (f) the gas diffusion and catalyst layers of the cathode.

use of novel architectures with the most uniformity of the reaction surface to decrease the maximum temperature in the fuel cell and increase net power.

4. Conclusions

In the present papera numerical analysis of three new tubular PEM fuel cell architectures namely: circular, square and triangular has been done for the first time. A summary of the results are presented below:

(a) Comparing the polarity curves indicated that circular and square tubular configurations propose higher current density compared to the base PEM fuel cell model. But the triangular tubular configuration shows a drop in current density, especially in the low-voltages, in comparison with the base PEM fuel cell model.

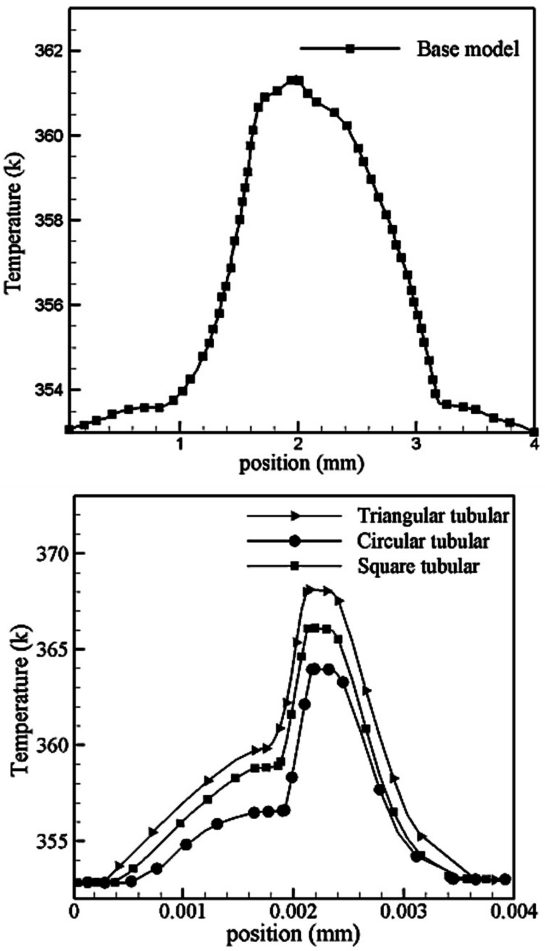

Fig.10. Lateral temperature distribution in the entrance region for (a) base modeland (b) three new tubular models.

(b) Circular tubular architecture indicated more uniform distribution for oxygen and hydrogen mass fraction contours in comparison with the two other architectures and especially with the triangular tubular architecture. Triangular architecture due to its low angle corners prevented uniform reaction so that the range of values in the catalyst and gas diffusion layers was wider. The maximum values existed on the corners, and the species values decreases and distribution becomes more uniform the further you moved from the corners.

(c) Water mass fraction contours in gas diffusion and the catalyst layers showed that by moving along the channel the water amount gradually increases. Like the previous contours, the triangular tubular showed the most uniformity in water distribution. A small amount of water content was predicted in the corners of this architecture indicating the slowness of the reaction in these regions. Unlike that case, the circular figure demonstrated a uniform distribution of the exit water vapor due to the uniform distribution of the species. Square architecture power production is placed between the circular and triangular architectures .

(d) Temperature distribution contours in gas diffusion and the catalyst layers at the cathode indicated that rising temperature is concentrated away from of the corner regions of the square and triangular architectures due to their sharp angles and slowness of reaction Furthermore, the centralized distribution of temperature rise increased the maximum temperature in limited regions for these two architectures. In the Circular architecture, due to the dispersion of reaction at all surfaces, distribution of rising temperature occurred in wider surfaces and therefore the maximum temperature for this architecture is low. But triangular geometry, due to its non-uniform reaction, has the maximum temperature compared with the two other architectures. This damages the catalyst and diffusion layers which results in an undesirable increase in cost especially for the catalyst layer. So this point should be considered when designing novel high temperature

fuel cells and designers should attempt to use novel figures with the highest level reaction as much as possible to increase power and decrease maximum temperature in fuel cell surfaces.

Acknowledgment

The authors are grateful to Iran Renewable Energy Organization (SUNA) for its financial support.

Nomenclature

$A_{a,c}$	Area cross section channel for anode and cathode	(m^2)
A_{mem}	Active cell area	(m^2)
a	Water activity	-
D	Mass diffusion coefficient	(m^2/s)
F	Faraday's constant	$(C/mole)$
K	Permeability	$(1/m^2)$
k	Thermal conductivity	(W/mk)
M	Molecular weight	$(g/mole)$
p	pressure	(Pa)
R	Universal gas constant	$(J/kg.mole)$
T	Temperature	(K)
V_{oc}	Open circuit voltage	(V)
X	Mole fraction	-

Greek symbols

α	Water transfer coefficient	-
ε	porosity	-
ρ	density	(Kg/m^3)
γ	Concentration coefficient	-
μ	Viscosity	
σ	membrane conductivity	$(1/ohm.m)$
λ	water content	-
ξ	stoichiometric ratio	-

Subscripts and Superscripts

an	anode	-
cat	cathode	-
eff	effective	-
mem	membrane	-
m	mass	-
i	individual specie in the reference condition	-
ref	reference value	-

5. References

[1] BARBIR, F. PEM Fuel cells. In: L. SAMMES, ed. Fuel Cell Technology: Reaching Towards Commercialization. Springer, Germany, 2007, 27-51.

[2] LUM, K. W. "Three-dimensional computational modelling of a polymer electrolyte membrane fuel cell" Thesis submitted in partial fulfillment for the award of Degree of Doctor of Philosophy of Loughborough University, UK, Unpublished, 2003.

[3] LARMINIE, J. and DICKS, A. "Fuel Cell Systems Explained".2nded. John Wiley & Sons Ltd, England, 2003. 75-79.

[4] YUAN, W., TANG, Y., PAN, M., LI, Z. and TANG, B. "Model prediction of effects of operating parameters on proton exchange membrane fuel cell performance". Renewable Energy, 2010, 35, 656-666.

[5] Alhazmi, N., D. B. Ingham, M. S. Ismail, K. J. Hughes, L. Ma, and M. Pourkashanian. "Effect of the anisotropic thermal conductivity of GDL on the performance of PEM fuel cells." International Journal of Hydrogen Energy, 2013, 38(1), 603-611.

[6] Jeon, Dong Hyup, Kwang Nam Kim, Seung Man Baek, and Jin Hyun Nam. "The effect of relative humidity of the cathode on the performance and the uniformity of PEM fuel cells." international journal of hydrogen energy, 2011, 36, (19), 12499-12511.

[7] Larbi, Badreddine, et al. "Effect of porosity and pressure on the PEM fuel cell performance." International Journal of Hydrogen Energy, 2013, 38(20), 8542-8549.

[8] Misran, Erni, NikSuhaimi Mat Hassan, Wan Ramli Wan

Daud, Edy Herianto Majlan, and Masli Irwan Rosli. "Water transport characteristics of a PEM fuel cell at various operating pressures and temperatures." International Journal of Hydrogen Energy, 2013, 38(22), 9401-9408.

[9] Ismail, M. S., K. J. Hughes, D. B. Ingham, L. Ma, and M. Pourkashanian. "Effects of anisotropic permeability and electrical conductivity of gas diffusion layers on the performance of proton exchange membrane fuel cells." Applied Energy 2012, 95, 50-63.

[10] Nabovati, Aydin, James Hinebaugh, Aimy Bazylak, and Cristina H. Amon. "Effect of porosity heterogeneity on the permeability and tortuosity of gas diffusion layers in polymer electrolyte membrane fuel cells." Journal of Power Sources 2014, 248, 83-90.

[11] Carcadea, Elena, D. B. Ingham, I. Stefanescu, R. Ionete, and H. Ene. "The influence of permeability changes for a 7-serpentine channel pem fuel cell performance." international journal of hydrogen energy 2011, 36(16), 10376-10383.

[12] Berning, T., and N. Djilali. "Three-dimensional computational analysis of transport phenomena in a PEM fuel cell—a parametric study." Journal of Power Sources 2003, 124(2), 440-452.

[13] Ahmed, Dewan Hasan, and Hyung Jin Sung. "Effects of channel geometrical configuration and shoulder width on PEMFC performance at high current density." Journal of Power Sources 2006, 162(1), 327-339.

[14] Yan, Wei-Mon, Hui-Chung Liu, Chyi-Yeou Soong, Falin Chen, and C. H. Cheng. "Numerical study on cell performance and local transport phenomena of PEM fuel cells with novel flow field designs." Journal of Power Sources 2006, 161(2), 907-919.

[15] Fontana, Éliton, Erasmo Mancusi, Adriano Da Silva, Viviana Cocco Mariani, Antonio Augusto Ulson De Souza, and Selene MA Guelli Ulson de Souza. "Study of the effects of flow channel with non-uniform cross-sectional area on PEMFC species and heat transfer." International Journal of Heat and Mass Transfer 2011, 54 (21), 4462-4472.

[16] Perng, Shiang-Wuu, and Horng-Wen Wu. "A three-dimensional numerical investigation of trapezoid baffles effect on non-isothermal reactant transport and cell net power in a PEMFC." Applied Energy 2015, 143, 81-95.

[17] Al-Baghdadi, Maher AR Sadiq. "Studying the effect of material parameters on cell performance of tubular-shaped PEM fuel cell." Energy Conversion and Management 2008, 49(11), 2986-2996.

[18] Sierra, J. M., S. J. Figueroa-Ramírez, S. E. Díaz, J. Vargas, and P. J. Sebastian. "Numerical evaluation of a PEM fuel cell with conventional flow fields adapted to tubular plates." International Journal of Hydrogen Energy 2014, 39(29) 16694-16705.

[19] Torkavannejad, Ashkan, Hamidreza Sadeghifar, Nader Pourmahmoud, and Farzin Ramin. "Novel architectures of polymer electrolyte membrane fuel cells: Efficiency enhancement and cost reduction." International Journal of Hydrogen Energy 2015, 40(36), 12466-12477.

[20] Wang, Lin, Attila Husar, Tianhong Zhou, and Hongtan Liu. "A parametric study of PEM fuel cell performances." International Journal of Hydrogen Energy 2003, 28(11), 1263-1272.

[21] Ansys Fluent 14.0 Documentation, Fluent Inc., 2010.

[22] Um, Sukkee, C-Y. Wang, and K. S. Chen. "Computational fluid dynamics modeling of proton exchange membrane fuel cells." Journal of the electrochemical society 2000, 147(12), 4485-4493.

[23] Parthasarathy, Arvind, Supramaniam Srinivasan, A. John Appleby, and Charles R. Martin. "Temperature dependence of the electrode kinetics of oxygen reduction at the platinum/Nafion® interface—a microelectrode investigation." Journal of the Electrochemical Society 1992, 139(9), 2530-2537.

[24] Springer, Thomas E., T. A. Zawodzinski, and Shimshon

Gottesfeld. "Polymer electrolyte fuel cell model." Journal of the Electrochemical Society 1991, 138(8), 2334-2342.

[25] Chippar, Purushothama, O. Kyeongmin, Kyungmun Kang, and HyunchulJu. "A numerical investigation of the effects of GDL compression and intrusion in polymer electrolyte fuel cells (PEFCs)." international journal of hydrogen energy 2012, 37(7), 6326-6338.

[26] Versteeg, HenkKaarle, and Weeratunge Malalasekera. An introduction to computational fluid dynamics: the finite volume method. Pearson Education, 2007.